Circadian Vesicle Capture and Phase-Delayed Activity Maximize Synaptic Neuropeptide Release by Clock Neurons

Markus K. Klose[1], Junghun Kim[1], Sydney N. Gregg[1], Brigitte F. Schmidt[2], Xiju Xia[3,4], Yulong Li[3,4], and Edwin S. Levitan[1]*

[1] Department of Pharmacology and Chemical Biology, University of Pittsburgh, Pittsburgh, PA 15261, USA

[2] Department of Chemistry, Carnegie Mellon University, Pittsburgh, PA, 15213, USA

[3] State Key Laboratory of Membrane Biology, School of Life Sciences, Peking University, Beijing 100871, China

[4] PKU-IDG/McGovern Institute for Brain Research, Beijing 100871, China

*Corresponding author: elevitan@pitt.edu

Classification:

major: Biological Sciences

minor: Neuroscience

Key words: clock neurons, presynaptic Ca^{2+}, GRAB sensor, peptidergic transmission, vesicle capture

25 pages

7 figures

The authors declare no competing interests.

Abstract

Drosophila **sLNv clock neurons release the neuropeptide PDF to control circadian rhythms. Strikingly, PDF content in sLNv terminals is rhythmic with late night synaptic accumulation occurring in preparation for exocytosis from dense-core vesicles (DCVs) hours later at midmorning. The timing of this rhythm has been puzzling because (a) DCV exocytosis occurs hours after elevations in resting membrane potential (RMP) and Ca^{2+} levels in the soma, which have traditionally been considered surrogates for activity and peptidergic transmission, and (b) the mechanism for the daily surge in synaptic neuropeptide content is unknown. Here, a sensor for sNPF, a neuropeptide co-packaged into DCVs along with PDF, reveals native synaptic neuropeptide release requires Ca^{2+} influx and occurs at midmorning under control of the circadian clock. Furthermore, Ca^{2+} imaging demonstrates that presynaptic activity and neuropeptide release both peak at the same time of day, showing that activity and release rhythms at the presynapse are remarkably uncoupled from somatic Ca^{2+} and RMP rhythms in these neurons. Finally, anterograde axonal transport of DCVs is constant throughout the day and retention of circulating DCVs rhythmically boosts presynaptic neuropeptide content. This late-night vesicle capture requires the circadian clock. Thus, the robust daily rhythms of synaptic neuropeptide release that controls circadian behavior is produced by clock-induced late-night vesicle capture and midmorning activity.**

Significance statement

Activity-dependent neuropeptide release from clock neuron distal terminals regulates behavioral biorhythms. Neuropeptide levels in fly sLNv clock neuron terminals cycle each day: they increase late at night and decrease hours later apparently due to dense-core vesicle exocytosis that is curiously delayed relative to daily somatic depolarization and Ca^{2+} elevation. Imaging shows that the boost in presynaptic neuropeptide content is mediated by circadian capture of release competent vesicles. Then at midmorning, long after presumptive somatic surrogates change, Ca^{2+} influx evokes native synaptic neuropeptide release. These results demonstrate a remarkable uncoupling of the daily rhythms in peptidergic synaptic transmission and somatic indices. Furthermore, the rhythmic burst of neuropeptide release controlling circadian behavior is produced by clock-controlled vesicle capture and phase-delayed activity.

Introduction

Drosophila sLNv neurons release the neuropeptide Pigment Dispersing Factor (PDF) to synchronize molecular rhythms of many individual neurons in the clock circuit to maintain daily rhythms in locomotor activity (Yoshii *et al.*, 2009; Helfrich-Forster and Reinhard, 2025). Interestingly, PDF content in sLNv neurons is rhythmic (Park *et al.*, 2000) with a drop in presynaptic PDF at midmorning that has been accounted for by Ca^{2+} influx-induced dense-core vesicle (DCV) exocytosis (Klose *et al.*, 2021; Ispizua *et al.*, 2024). Furthermore, rhythmic exocytosis is preceded by an hours long accumulation in terminal neuropeptide content (Park *et al.*, 2000; Klose *et al.*, 2021), which is advantageous because release scales with presynaptic neuropeptide content (Bulgari et al., 2014; Cavolo et al., 2016). The basis of the daily increase in presynaptic PDF content has not been determined, although a role for PDF gene expression has been excluded (Park *et al.*, 2000). Furthermore, the timing peak of daily DCV exocytosis rhythms at sLNv terminals, which was determined with an exogenously expressed neuropeptide tagged with a fluorogen-activating protein (Dilp2-FAP, Bulgari *et al.*, 2019; Klose *et al.*, 2021), is curious because release occurs hours after daily rises in somatic resting membrane potential (RMP) and intracellular Ca^{2+} (Cao and Nitabach, 2008; Liang *et al.*, 2016), which are typically considered to be indicative of axonal electrical activity and synaptic transmission. Notably, even though clock-driven ion channel expression is crucial for clock neuron function (Ruben *et al.*, 2012; Flourakis *et al.*, 2015), daily rhythms in activity and the resultant presynaptic Ca^{2+} transients that evoke neuropeptide release have not been measured in sLNv neurons. Therefore, the rhythms in synaptic neuropeptide accumulation and release by sLNv clock neurons are not

understood.

Here, we determine the mechanism underlying the increase in synaptic neuropeptide content in preparation for release and address the different timing of synaptic release and somatic physiology. First, a recently developed GPCR-based sensor for sNPF (Xia and Li, 2024), a neuropeptide co-packaged with PDF into sLNv neuron DCVs (Yu *et al.*, 2024), is used to elucidate the daily timing of native neuropeptide release. Second, the timing of synaptic neuropeptide release is shown to match rhythmic activity as revealed by presynaptic Ca^{2+} imaging rather than somatic changes in RMP and Ca^{2+}. Finally, axonal DCV transport is studied to determine how the daily increase on synaptic neuropeptide content occurs. Together, imaging of sLNv neuron axons and terminals shows that the circadian clock induces synaptic capture of DCVs late at night to build up neuropeptide content so that hours later at midmorning activity elicits a maximal daily burst of neuropeptide release.

Results

The daily burst of synaptic neuropeptide release by sLNv neurons

sLNv somatic Ca^{2+} and RMP, which have been presumed to be surrogates electrical activity and synaptic transmission, rise together by sunrise (Cao and Nitabach, 2008; Liang *et al*., 2016). Yet, synaptic exocytosis of DCVs, as measured by cumulative fusion pore opening events detected with Dilp2-FAP, depends on Ca^{2+} influx and peaks hours later (Klose *et al.*, 2021). A potential explanation for the mismatched timing of somatic physiology and synaptic DCV exocytosis is that Dilp2-FAP, an exogenous neuropeptide-based indicator, might not reflect the exocytosis of native neuropeptide-

containing DCVs. Two recent developments suggested that this hypothesis could be tested by measuring endogenous neuropeptide release by sLNv terminals. First, PDF was found to be co-packaged with another neuropeptide (sNPF) in the same individual DCVs in sLNv neurons (Yu *et al.*, 2024). Second, a new GPCR-activation-based sensor for detecting sNPF ($GRAB_{sNPF1.0}$) was developed (Xia and Li, 2024). Therefore, $GRAB_{sNPF1.0}$ expression was driven in LNv neurons with PDF-GAL4 and the neurons were imaged in brain explants.

Based on Xia and Li (2024), validation experiments included demonstrating dose-dependent responses to *Drosophila* sNPF2 (Fig. 1A). We then tested for a daily rhythm in $GRAB_{sNPF1.0}$ signals at sLNv terminals, an expected site of sNPF release. These experiments showed that the peak sNPF signal occurs at ZT 3 (Fig. 1B), which coincides with peak exocytosis from DCVs measured with Dilp2-FAP (Klose *et al.*, 2021). This peak cannot be attributed to a change in sensor expression because Fmax values do not change between ZT 23 and ZT 3 (Fig. 1C). Selective knockdown of sNPF expression in sLNv neurons by RNA interference (RNAi) reduced $GRAB_{sNPF1.0}$ fluorescence at ZT 3 (Fig. 1D) revealing daily peaks in sNPF sensor fluorescence are the result of neuropeptide release from sLNv neurons and not other sNPF-expressing neurons (Fig. 1D). Furthermore, application of 100 μM Cd^{2+} inhibited the ZT 3 signal (Fig. 1E) showing that Ca^{2+} influx is required. Finally, consistent with the control of daily neuropeptide rhythms by the circadian clock, the elevated sNPF sensor signal at ZT 3 was lost in the per^{01} (Park *et al.*, 2000) clock gene amorphic mutant (Fig. 1F). Therefore, together the above experiments show that Ca^{2+} influx-evoked endogenous neuropeptide release by sLNv synapses is triggered by the clock hours after the

increases in somatic Ca^{2+} and RMP occur.

Ca^{2+} rhythms in sLNv terminals

These results led us to hypothesize that the presynaptic Ca^{2+} influx induced by activity and resultant synaptic neuropeptide release are not reflected by RMP and intracellular Ca^{2+} levels measured at the soma. This is possible, although not usually presumed, for a number of reasons. First, action potentials are attenuated in the *Drosophila* neuronal soma because their initiation zone is distally located and backpropagation to the soma is passive (Ravenscroft *et al.*, 2020). Thus, any coupling of activity-induced Ca^{2+} influx between the soma and terminals could be weak. Also, a prior electrophysiology study at sLNv somas did not address whether there is a daily rhythm in the frequency of attenuated somatic action potentials, but only reported daily changes in somatic RMP (Cao and Nitabach, 2008). Therefore, it remains unclear that rhythmic changes in somatic RMP are sufficient to drive the axonal activity that in turn evokes synaptic neuropeptide release. Third, intracellular Ca^{2+} channels such as the IP_3R signal daily in the soma without altering synaptic release by LNv neurons (Klose *et al.*, 2021). This implies that Ca^{2+} measured at the soma does not necessarily reflect Ca^{2+} influx at the presynapse that triggers DCV-mediated release. These concerns led us to study presynaptic Ca^{2+} at different times of the day with cytoplasmic GCaMP8f or synaptotagmin-fused synapse-targeted GCaMP8f, which resolves Ca^{2+} transients evoked by individual action potentials in *Drosophila* synaptic boutons (Li *et al.*, 2021).

In the morning, sLNv terminal imaging experiments with either GCaMP8f version revealed spontaneous presynaptic fast Ca^{2+} transients that display a rapid rise (< 55

ms) and subsequent slower decay (Fig. 2) as expected for synaptic action potential responses (Li *et al.*, 2021). Also consistent with activity responses, the transients are blocked by the Cd^{2+} application, thereby showing that they require Ca^{2+} influx (Fig. 2A). We then determined the daily timing of spontaneous activity. Strikingly, the frequency of activity varies across the day with a peak of 2.4 $\pm$ 0.3 Hz at ZT 3 (Fig. 2B), which corresponds to the timing of peak synaptic neuropeptide release (Fig. 1B) and DCV exocytosis (Klose *et al.*, 2021), and a nadir at night when the firing was not statistically different from 0 Hz (ZT 21, P = 0.4; ZT 23, P = 0.18). These Ca^{2+} imaging data lead to two conclusions. First, the matched timing of activity, DCV exocytosis and sNPF release implies that synaptic Ca^{2+} channel activity triggers the midmorning burst of synaptic neuropeptide release by sLNv terminals. Second, since presynaptic activity occurs hours after observed changes in somatic Ca^{2+} and RMP (Cao and Nitabach, 2008; Liang *et al*., 2016), those somatic physiological indicators do not govern activity at the presynapse.

Because synaptic neuropeptide release is limited to the peak of activity, we considered why lower frequency activity prior to the peak did not elicit neuropeptide release. First, peak activity might simply be needed for efficient release because of the superlinear dependence of release on Ca^{2+}. Alternatively, the lower activity prior to the peak may not evoke synaptic release because recently accumulated neuropeptide is in DCVs that are not yet competent for release (i.e., because they require priming). To test the latter hypothesis, the DCV exocytosis response to K^{+}-induced depolarization was measured with Dilp2-FAP imaging (Bulgari *et al.*, 2019) at ZT 1, a time point when neuropeptide content has already increased, but daily exocytosis has not yet been

initiated (Klose *et al.*, 2021). Strikingly, DCV exocytosis in response to depolarization, as revealed with the membrane impermeant fluorogen MG-Tcarb, is robust at ZT 1 (Fig. 3, Hi K^+). Furthermore, the release evoked by depolarization at ZT 1 is comparable to peak endogenous release at ZT 3 (Klose et al., 2021), suggesting that endogenous rhythmic release depletes the releasable pool. To relate release to the total presynaptic pool, a membrane permeant version of the fluorogen (MGnBu, Perkins *et al.*, 2018) was applied to label presynaptic Dilp2-FAP. This showed that the releasable pool was about half of the total neuropeptide pool in terminals (Fig. 3, MGnBu). Thus, at ZT 1 there is a large pool of release-competent DCVs in sLNv terminals. Therefore, the timing of release is not due to a change in vesicle releasability, but instead reflects the requirement for peak activity to elicit robust synaptic neuropeptide release.

DCV capture produces the daily accumulation of presynaptic neuropeptide content

We then shifted to studying the accumulation of presynaptic neuropeptide in preparation for release. To test the hypothesis that increased delivery of DCVs to sLNv terminals produces the daily upregulation of presynaptic neuropeptide content, axonal transport of DCVs was imaged in brain explants isolated at different times of the day from PDF>Dilp2-GFP (UAS-Dilp2-GFP; PDF-GAL4) flies. Initially, the ratio of anterograde DCV flux to retrograde DCV flux (A/R) was measured from kymographs (Fig. 4A,B). These experiments showed that the flux ratio changed ($P < 0.001$, one-way ANOVA) with a peak late at night (i.e., at ZT 23) (Fig. 4B,C), a time when *Drosophila* display morning anticipation and PDF is accumulating in sLNv terminals in preparation for subsequent release. Thus, there is a net increase in axonal transport of DCVs to

sLNv terminals hours before the burst of release.

Anterograde and retrograde DCV transport were then examined individually to determine which component of the flux ratio changed, the numerator (A) or the denominator (R). Analysis of axonal transport showed that anterograde DCV flux (A) was constant at all times tested (Fig. 5A), thus ruling out rhythmic changes in the ratio being driven by anterograde axonal transport from the soma. Rather, retrograde axonal DCV flux (R) cycled ($P < 0.01$, one-way ANOVA) with a minimum late at night at ZT 23 (Fig. 5B). This drop in retrograde flux cannot be explained by exocytosis-induced DCV depletion since the flux drop precedes daily synaptic neuropeptide release by several hours (Klose *et al.*, 2021; Fig. 1B). Importantly, this drop in retrograde transport occurs at a time when there are no Ca^{2+} influx transients (Fig 2B) showing that this effect is independent of activity. Furthermore, the decrease in retrograde flux occurred without altering the velocity of DCVs undergoing retrograde axonal transport (Fig. 5C), thus excluding a slowing of the retrograde transport motors. Therefore, as demonstrated previously (Shakiryanova *et al.*, 2006; Wong *et al.*, 2012), the observed reduction in retrograde flux while there is no ongoing release is indicative of increased synaptic capture of circulating DCVs. Hence, increased DCV capture, as opposed to greater DCV delivery, produces the daily increase in synaptic neuropeptide content.

Late night vesicle capture requires the circadian clock

Rhythmic changes in presynaptic neuropeptide content (Park *et al.*, 2000) overlap with morphological plasticity in the sLNv axonal arbor (Fernandez *et al.*, 2008). To probe whether presynaptic DCV capture and axonal morphology are linked, DCV

axonal transport was studied in a PDF receptor (PDFR) null mutant (*han*), which prevents daily changes in terminal morphology while preserving rhythmic changes in PDF (Herrero *et al.*, 2020). In PDFR null animals, which lose synchronization of many clock neurons while cell autonomous clock function is maintained (Collins *et al.*, 2014; Helfrich-Forster and Reinhard, 2025), the daily rhythmic changes in axonal flux ratio persisted (Fig. 6A). Therefore, the daily rhythm in DCV capture occurs independently of PDFR expression and the accompanying morphological plasticity it drives.

The PDFR null mutant also abolishes morning anticipation behavior (i.e., the increase in motor activity prior to sunrise) (Hyun *et al.*, 2005). Because rhythmic capture occurs concurrently with this clock-dependent increase in locomotor behavior but persists when it is disrupted by the PDFR null mutation, we considered whether capture depends on the circadian clock. If capture is independent of the circadian clock, rhythmic capture would likely be driven through environmental cues, namely daily changes in light levels, and thus would be disrupted after shifting to constant conditions. However, after shifting to constant darkness (DD) capture remained different between CT23 and CT3 (Fig. 6B, CON). To further test for a role of the circadian clock, we examined the effect of a null mutation in the *period* gene (per^{01}), which is a critical component of the molecular clock itself, under DD conditions. Consistent with the loss of oscillation in synaptic PDF content with this mutant (Park *et al.*, 2000), the difference in capture under DD conditions was disrupted in per^{01} animals (Fig. 6C). Therefore, rhythmic DCV capture depends on the circadian clock. This effect cannot be a secondary response to clock-induced activity and neuropeptide release because capture occurs hours before the rhythmic increases in activity and synaptic release

occur. Thus, the clock induces sequential DCV capture and neuropeptide release.

Discussion

PDF release from sLNv neurons regulates circadian locomotor activity. It has long been known that PDF levels are rhythmic (Park *et al.*, 2000), but how these daily changes arose was poorly understood. Specifically, daily rhythms in somatic RMP and Ca^{2+} (Cao and Nitabach, 2008; Liang *et al*., 2016) are unexpectedly desynchronized from synaptic DCV exocytosis rhythms (Klose et al., 2021), and the basis for the late-night rise in presynaptic neuropeptide content was unknown. Here, imaging native neuropeptide levels, presynaptic Ca^{2+} and axonal DCV transport demonstrate that the daily changes in presynaptic neuropeptide levels are produced by rhythmic DCV capture elicited by the circadian clock and subsequent phase-delayed activity-induced neuropeptide release (Fig. 7).

The timing differential between daily vesicle capture and activity in sLNv terminals is striking. The timing of rhythmic vesicle capture is shown here to be driven by the circadian clock (Fig. 6B), and occurs hours after synaptic activity has concluded for the day (Fig. 2B). Such constitutive vesicle capture, which has been studied with a specialized photobleaching method and cell biological approaches that are problematic to apply in the brain, reflects local presynapse microtubule dynamics (Wong et al., 2012; Guedes-Dias et al., 2019; Aiken and Holzbaur, 2024). Vesicle capture in the sLNv terminals is induced independently of concurrent axonal arbor plasticity (Fig. 6A), a daily morphology change based on small G proteins, which is also controlled by the clock (Petsakou *et al.*, 2015; Gundermann *et al.*, 2023). In addition to vesicle capture and

morphological plasticity, the clock drives rhythmic electrical activity in *Drosophila* clock neurons by regulating K^+ channel gene expression and traffic of a Na^+ channel to the plasma membrane (Ruben *et al.*, 2012; Flourakis *et al.*, 2015). Given the diverse cell biological mechanisms involved, it is likely that the multiple cell biological outputs of the clock are induced with varying kinetics. Specifically, the results presented here suggest that the clock changes the dynamics of already existing microtubules much more quickly than expression and targeting of ion channels. This timing disparity is further amplified by the requirement for peak activity to evoke synaptic neuropeptide release by sLNv terminals. Because release scales with presynaptic neuropeptide content (Bulgari et al., 2014; Cavolo et al., 2016), leveraging the differential timing of clock outputs to first induce capture of release competent DCVs and then phase-delayed activity maximizes the daily burst of synaptic neuropeptide release from sLNv clock neurons that promotes synchronization of clock circuit neurons.

The current study demonstrates that Ca^{2+} channel activity and resultant neuropeptide release at the sLNv presynapse are not directly timed by RMP and Ca^{2+} levels in the soma. This likely reflects limited electrical coupling between the soma and the distal axonal segment (DAS), where action potentials initiate in *Drosophila* neurons (Ravenscroft *et al.*, 2020), and confounding changes in somatic Ca^{2+} by activity-independent mechanisms (e.g., IP_3R activation) (Klose *et al.*, 2021). Interestingly, preferential clock-driven upregulation of channels that preferentially localize in the DAS rather than in the sLNv soma could produce the disparity between the soma and terminals. Given that many studies use somatic physiological measurements as surrogates for activity and synaptic transmission, the disparity shown here between

compartments in sLNv neurons illustrates the need to fully characterize soma-terminal physiological coupling in order to properly deduce connectivity in neural circuits from soma-derived data.

Materials and methods

Physiology: All flies were entrained for at least for 72 hours in a 12-hour light: 12-hour dark (LD) schedule before dissection of 4-9 day old males to generate brain explants. Dissections during the dark phase were performed under a red light. Adult flies were immobilized with CO_2 gas and brains were dissected in 0 Ca^{2+} HL3 saline solution (70 mM NaCl, 5 mM KCl, 20 mM $MgCl_2$*$6H_2O$, 115 mM Sucrose, 5 mM Trehalose, 5 mM Hepes, and 10 mM $NaHCO_3$, pH 7.3) and then put into polylysine-coated plastic dishes containing HL3 with 2 mM Ca^{2+} for imaging (Klose et al., 2016). High potassium (Hi K+) saline was used to elicit neuropeptide release (35 mM NaCl, 80 mM KCl, 10 mM $MgCl_2$*$6H_2O$, 65 mM Sucrose, 5 mM Trehalose, 5 mM Hepes, and 10 mM $NaHCO_3$, pH 7.3).

All imaging was done on setups with an upright Olympus microscope equipped with a 60× 1.1 NA dipping water immersion objective, a Yokogawa spinning disk confocal head, a 488 nm laser for GFP illumination, a 561 nm laser for mScarlet3 detection, a 640 nm laser for FAP imaging, and a Teledyne Photometrics sCMOS camera.

Two fluorescent probes were expressed using the PDF-GAL4 driver to image neuropeptide release from sLNv terminals is the dorsal protocerebrum. The first was the sNPF sensor, $GRAB_{sNPF1.0}$ (Xia and Li, 2024), and the other was Dilp2-FAP (Bulgari *et*

al., 2019), which detects fusion pore opening events. UAS-GRAB$_{sNPF1.0}$ expression in sLNv terminals was used to detect both sNPF endogenous release and application of exogenous sNPF2 (GenScript). FAP imaging experiments were performed as previously described (Klose *et al.*, 2021). In the current experiments, a recombinant with UAS-Dilp2-GFP (Wong *et al.*, 2012) and UAS-Dilp2-FAP was used so that GFP could be used for focusing before application of the fluorogens MG-Tcarb (membrane impermeant) or MGnBu (membrane permeant) (Perkins *et al.*, 2018). Ca^{2+} imaging with UAS-GCaMP8f or UAS-syt-mScarlet3-GCaMP8f (Li *et al.*, 2021) driven by PDF-GAL4 was done at 18 Hz. Quantification of fluorescence was done in Imagej or Fiji. Statistical analysis was performed with Graphpad Prism software.

For DCV axonal transport, two axonal regions in the dorsal protocerebrum were imaged in each hemisphere of the brain. Time-lapse experiments entailed acquiring 180 images with 150 ms exposure times at 3 Hz. From these movies, regions where dorsally projecting axons defasciculated from bundles were used for generating kymographs with the Kymograph plugin of ImageJ.

Fly lines: All flies used the PDF-Gal4 promoter on the third chromosome (provided by Paul Taghert, Washington University in St. Louis). PDF-GAL4 drives expression in the two subsets of clock neuron that express PDF neuropeptide, the small ventrolateral (sLNv) neurons and the large ventrolateral (lLNv) neurons, of which only the sLNv neurons express sNPF. UAS-Dilp2-GFP, UAS-Dilp2-FAP, UAS- GRAB$_{sNPF1.0}$ and UAS-synaptotagmin-mScarlet3-GCaMP8f flies were reported previously (Wong *et al.*, 2012; Bulgari *et al.*, 2019; Li *et al.*, 2021; Xia and Li, 2024). w^{1118} flies were from Zachary

Freyberg (University of Pittsburgh). All other lines were from the Bloomington *Drosophila* stock center including *Bl#* 92857 (UAS-GCaMP8f), *Bl#* 33068 (*han*), *Bl#* 35785 (UAS-mCherry RNAi), and *Bl#* 80917 (per^{01}).

Funding

This research was supported by National Institutes of Health grant R01NS032385 to ESL.

Acknowledgments

We thank Paul Taghert (Washington University in St. Louis) for the PDF-GAL4 (III) flies and Dion Dickman (USC) for the UAS-synaptotagmin-mScarlet3-GCaMP8f flies. Stocks obtained from the Bloomington Drosophila Stock Center (NIH P40OD018537) were used in this study. We are also thankful for suggestions from Marcel Bruchez (Carnegie Mellon University, deceased) and comments on the manuscript from David Deitcher (Cornell University).

References

Aiken J, Holzbaur ELF. Spastin locally amplifies microtubule dynamics to pattern the axon for presynaptic cargo delivery. Curr Biol. 2024;34(8):1687-1704.e8.

Bulgari D, Zhou C, Hewes RS, Deitcher DL, Levitan ES. Vesicle capture, not delivery, scales up neuropeptide storage in neuroendocrine terminals. Proc Natl Acad Sci U S A. 2014;111(9):3597-601.

Cao G, Nitabach MN. Circadian control of membrane excitability in Drosophila melanogaster lateral ventral clock neurons. J Neurosci. 2008;28(25):6493-501.

Cavolo SL, Bulgari D, Deitcher DL, Levitan ES. Activity Induces Fmr1-Sensitive Synaptic Capture of Anterograde Circulating Neuropeptide Vesicles. J Neurosci. 2016;36(46):11781-11787.

Collins B, *et al*. Differentially timed extracellular signals synchronize pacemaker neuron clocks. Plos Biol. 2014;2(9):e1001959.

Fernández MP, Berni J, Ceriani MF. Circadian remodeling of neuronal circuits involved in rhythmic behavior. PLoS Biol. 2008;6(3):e69.

Flourakis M, Kula-Eversole E, Hutchison AL, Han TH, Aranda K, Moose DL, White KP, Dinner AR, Lear BC, Ren D, Diekman CO, Raman IM, Allada R. A Conserved Bicycle Model for Circadian Clock Control of Membrane Excitability. Cell. 2015;162(4):836-48.

Guedes-Dias P, Nirschl JJ, Abreu N, Tokito MK, Janke C, Magiera MM, Holzbaur ELF. Kinesin-3 Responds to Local Microtubule Dynamics to Target Synaptic Cargo Delivery to the Presynapse. Curr Biol. 2019;29(2):268-282.e8.

Gundermann DG, Lymer S, Blau J. A rapid and dynamic role for FMRP in the plasticity

of adult neurons. bioRxiv. 2023;doi:10.1101/2023.09.01.555985.

Helfrich-Forster C, Reinhard N. Mutual coupling of neurons in the circadian master clock: What we can learn from fruit flies. Neurobiol Sleep Circadian Rhythms. 2025; 18:100112.

Herrero A, Yoshii T, Ispizua JI, Colque C, Veenstra JA, Muraro NI, Ceriani MF. Coupling Neuropeptide Levels to Structural Plasticity in Drosophila Clock Neurons. Curr Biol. 2020;30(16):3154-3166.e4.

Hyun S, *et al.* Drosophila GPCR Han is a receptor for the circadian clock neuropeptide PDF. Neuron. 2005; 48(2):267-278.

Ispizua *et al.* Ultrastructural correlates of circadian structural plasticity. bioRxiv. 2024; doi:10.1101/2024.11.06.622332.

Klose MK, Bruchez MP, Deitcher DL, Levitan ES. Temporally and spatially partitioned neuropeptide release from individual clock neurons. Proc Natl Acad Sci U S A. 2021;118(17):e2101818118.

Klose MK, Duvall L, Li W, Liang X, Ren C, Steinbach J, Taghert P. Functional PDF Signaling in the Drosophila Circadian Neural Circuit Is Gated by Ral A-Dependent Modulation. Neuron. 2016;90(4):781-794.

Li X, Chien C, Han Y, Sun Z, Chen X, Dickman D. Autocrine inhibition by a glutamate-gated chloride channel mediates presynaptic homeostatic depression. Sci Adv. 2021;7(49):eabj1215.

Liang X, Holy TE, Taghert PH. Synchronous *Drosophila* circadian pacemakers display nonsynchronous Ca^{2+} rhythms *in vivo*. Science. 2016; 351(6276):976-81.

Nitabach MN, Blau J, Holmes TC. Electrical silencing of Drosophila pacemaker neurons stops the free-running circadian clock. Cell. 2002;109(4):485-95.

Park JH, Helfrich-Förster C, Lee G, Liu L, Rosbash M, Hall JC. Differential regulation of circadian pacemaker output by separate clock genes in Drosophila. Proc Natl Acad Sci U S A. 2000;97(7):3608-13.

Perkins LA, Fisher GW, Naganbabu M, Schmidt BF, Mun, F, Bruchez MP. High-content surface and total expression siRNA kinase library screen with vx-809 treatment reveals kinase targets that enhance F508del-CFTR rescue. Mol Pharm 2018; 5(3):759-767.

Petsakou A, Sapsis TP, Blau J. Circadian rhythms in Rho1 activity regulate neuronal plasticity and network hierarchy. Cell. 12015; 62: 823–835.

Ruben M, Drapeau MD, Mizrak D, Blau J. A mechanism for circadian control of

pacemaker neuron excitability. J Biol Rhythms. 2012;27(5):353-64.

Shakiryanova D, Tully A, Levitan ES. Nat Neurosci. Activity-dependent synaptic capture of transiting peptidergic vesicles. 2006;9(7):896-900.

Wong MY, Shakiryanova D, Levitan ES. Presynaptic ryanodine receptor-CamKII signaling is required for activity-dependent capture of transiting vesicles. J Mol Neurosci. 2009;37(2):146-50.

Wong MY, Zhou C, Shakiryanova D, Lloyd TE, Deitcher DL, Levitan ES. Neuropeptide delivery to synapses by long-range vesicle circulation and sporadic capture. Cell. 2012;148(5):1029-38.

Xia X, Li, Y. A new GRAB sensor reveals differences in the dynamics and molecular regulation between neuropeptide and neurotransmitter release bioRxiv. 2024; doi: 10.1101/2024.05.22.595424.

Yoshii T, Wülbeck C, Sehadova H, Veleri S, Bichler D, Stanewsky R, Helfrich-Förster C. The neuropeptide pigment-dispersing factor adjusts period and phase of Drosophila's clock. J Neurosci. 2009;29(8):2597-610.

Yu J, Zhang Y, Clements K, Chen N, Griffith LC. Genetically-encoded markers for confocal visualization of single dense core vesicles. bioRxiv. 2024; doi: 2024.10.07.617131.

Figure Legends

Figure 1. Circadian rhythm of neuropeptide release from sLNv nerve terminals.

A. (i) $GRAB_{sNPF1.0}$ images in sLNv nerve terminals before (Pre) and after application of exogenous 3 μM sNPF2 to the brain explant. Shown images are maximum z-projections from image stacks made from 8 1 um steps. (ii) Dose-response curve for $GRAB_{sNPF1.0}$ in LNv neurons in response to various concentrations of sNPF2. Note that responses are expressed in fold change relative to initial fluorescence (F_0). B. Graph represents average $GRAB_{sNPF1.0}$ fluorescence from sLNv nerve terminals at different times of day (ZT) in flies entrained to a 12 hour light:12 hour dark cycle. One-way ANOVA revealed a significant difference ($P < 0.0001$). Post-test analysis by Tukey's multiple-comparison test is presented: ****$P < 0.0001$, ***$P < 0.001$. C. The maximal $GRAB_{sNPF1.0}$ response evoked by 3 μM (F_{max}) did not change between ZT 23 and ZT 3. D. $GRAB_{sNPF1.0}$ fluorescence at peak release time of day (ZT3) in the sLNv terminals of control UAS-$GRAB_{sNPF1.0}$; PDF-GAL4 flies (CON) and UAS-sNPF RNAi/UAS-$GRAB_{sNPF1.0}$; PDF-GAL4 flies (RNAi sNPF) (t-test, $P < 0.01$). E. $GRAB_{sNPF1.0}$ fluorescence at peak release time of day (ZT3) in the sLNv terminals 60 minutes after the application of vehicle or 100 μM cadmium chloride (Cd^{2+}) (t-test, $P < 0.05$). F. $GRAB_{sNPF1.0}$ fluorescence at peak release time of day (ZT3) in the sLNv terminals in controls and *per*^{01} (*per01*) flies (t-test, $P < 0.01$).

Figure 2. Presynaptic Ca^{2+} imaging in sLNv nerve terminals.

A. (i) Cytoplasmic GCaMP8F driven by PDF-GAL4 in distal sLNv nerve terminals

imaged over time at ZT 1. (ii) GCaMP8F fluorescence from one ROI measured at 18 Hz in normal HL3 saline. (iii) Graph represents GCaMP8F fluorescence from one ROI measured at 18 Hz ms in HL3 saline before and after adding 100 μM cadmium chloride (Cd^{2+}). (iv) Morning (ZT1-5) activity frequency of sLNv nerve terminals expressing GCaMP8F before and after Cd^{2+} (100 μM). (v) Morning (ZT1-5) activity frequency of sLNv nerve terminals expressing Syt-mScarlet3-GCaMP8F before and after Cd^{2+} (100 μM). Note that ZTs were not matched between iv and v. B. (i) Syt-mScarlet3-GCaMP8F traces in distal sLNv nerve terminals imaged over time at ZT 21, 1 and 3. Bar indicates 3 s. (ii) Average Ca^{2+} transient frequencies measured in sLNv nerve terminals at different times of day using Syt-mScarlet3-GCaMP8F. One-way ANOVA revealed a significant difference ($P < 0.0001$). Post-test analysis by Tukey's multiple-comparison test is presented: ****$P < 0.0001$, ***$P < 0.001$.

Figure 3. A large releasable pool of DCVs is present at ZT 1 in sLNv nerve terminals.

A. Confocal images of the FAP signal in sLNv terminals following one-hour exposure to MG-Tcarb in normal HL3 saline (CON), MG-Tcarb in high K^+ saline (Hi K+), or with exposure to the membrane permeant MG analog MGnBu (500nM) in normal HL3 saline. Scale bar is 10 μm. B. Quantification of FAP-MG fluorescence in sLNv nerve terminals exposed to MG-Tcarb in normal HL3 saline (CON), MG-Tcarb in Hi K+ HL3 saline, or membrane permeable MGnBu in normal HL3 saline. ***$P < 0.001$, *$P < 0.05$. n = 10 for CON; n = 9 for Hi K+; n = 6 for MGnBu. One-way ANOVA revealed a significant difference ($P < 0.001$). Post-test analysis by Tukey's multiple-comparison test is

presented: ***P < 0.001, *P < 0.05.

Figure 4. Dense-core vesicle flux in sLNv nerve terminal projections.

Ai. sLNv projections containing DCVs filled with Dilp2-GFP at t = 0.33 seconds of recording. White box reveals region of interest (ROI) for analysis. Aii. DCVs at t = 0, 0.33, 0.66, and 1.0 seconds (red arrow indicates anterograde (AR) transport and blue arrow indicates retrograde (RE) transport, scale bar = 1 μm). Aiii. Kymograph of ROI (red arrow anterograde, blue arrow retrograde transport). B. Kymographs reveal both anterograde (slope down, left to right) and retrograde (slope down, right to left) DCV axonal transport in sLNv projections of PDF>Dilp2-GFP flies at ZT 3 and ZT 23. C. Flux ratios (anterograde/retrograde) at different times of the day. n values (number of hemibrains) for ZT 0, 3, 5, 8, 11, 14, 17, 20, 21, 22, 23 are 4, 10, 6, 6, 8, 6 ,8, 8,12, respectively. One-way ANOVA revealed significant difference (P < 0.001). Post-test analysis by Dunnett's multiple-comparison test is presented: ****P < 0.0001, ***P < 0.001, *P < 0.05.

Figure 5. Dense-core vesicle flux and velocity in sLNv nerve terminal projections.

A. Anterograde flux and B. Retrograde flux (vesicles/min) in PDF>Dilp2-GFP brains. n values for ZT 2-4, 8-10, 14-16, and 23 are 11,12,10, and 9, respectively. P < 0.01, one-way ANOVA. **P < 0.01, Dunnett's multiple-comparison post-test. C. Retrograde velocity of DCVs at ZT 3 and 23 in PDF>Dilp2-GFP brains (left, average of each brain; ZT 3 n = 4, ZT 23 n = 4; right, average of all vesicles measured: ZT 3 n = 49, ZT 23 n = 51).

Figure 6. Dependence of rhythmic capture on the PDFR and *per*.

A. Ratios of anterograde to retrograde DCV flux (A/R) at ZT 3 and ZT 23 in *w*; UAS-Dilp2-GFP; PDF-GAL4 controls (CON) and *han*; UAS-Dilp2-GFP; PDF-GAL4 PDFR null (*han*) sLNv axons. n $\geq$ 13 for CON; n > 20 for *han*. For both CON and *han*, ****P < 0.0001, unpaired t-test. B. Ratios of anterograde to retrograde DCV flux (A/R) 2 days after transition to constant darkness at CT3 and CT23 in *w*; UAS-Dilp2-GFP; PDF-GAL4 controls (CON) and $y^1 per^{01} w^*$; *UAS-Dilp2-GFP; PDF-GAL4* (*per*) sLNv axons. n = 9 for CON; n = 6 for CT3 and n = 7 for CT23 in *per* animals. **P < 0.01, unpaired t-test.

Figure 7. Summary schematic of the timing of daily neuropeptide release.

The epoch of somatic RMP and Ca^{2+} is shown with the orange arc, while the timing of presynaptic fast Ca^{2+} transients is shown by the black arc. The timing of presynaptic DCV capture is indicated by the red arrow, while the timing of presynaptic DCV exocytosis and neuropeptide release is indicated by the blue arrow.

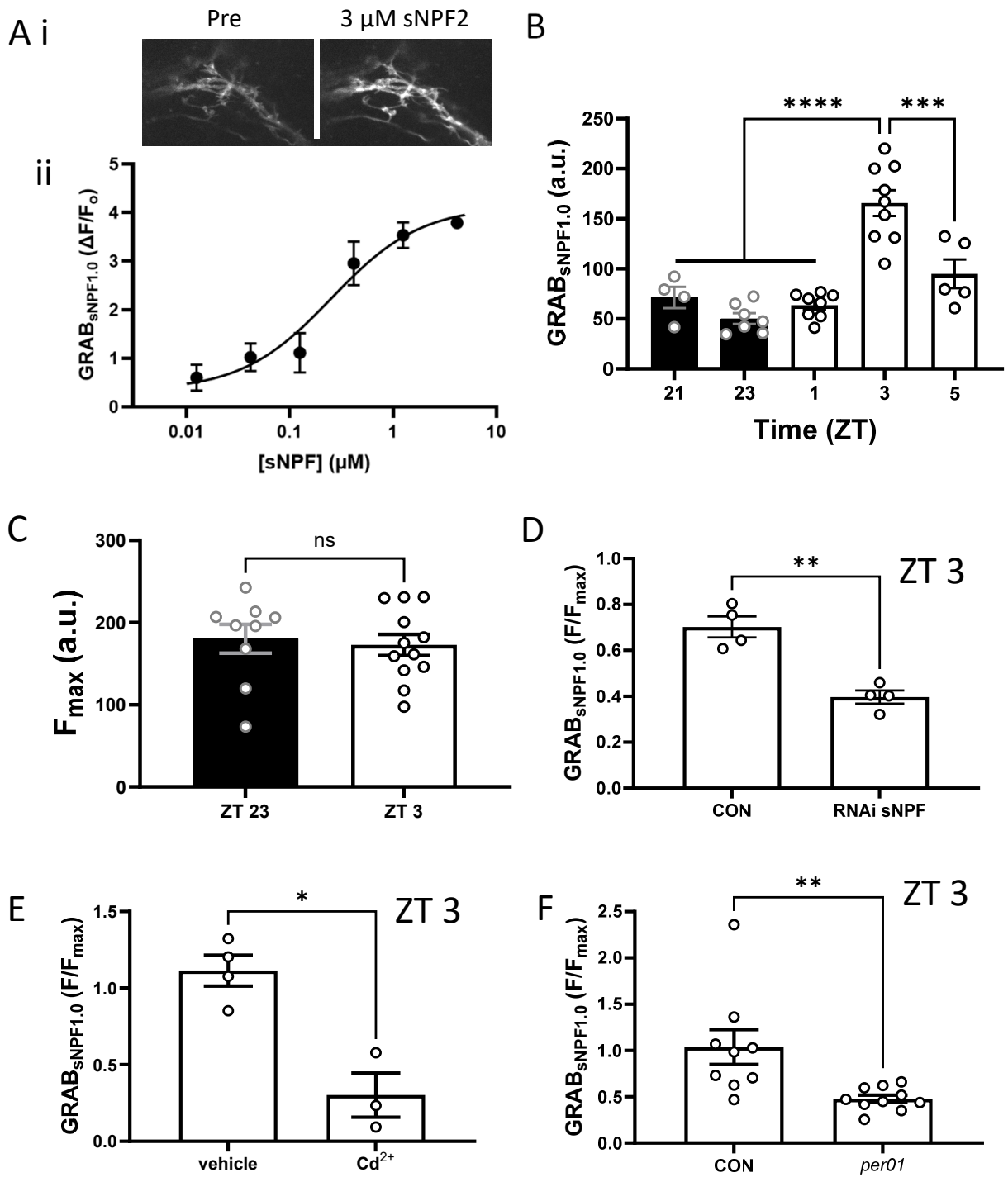
A i
Pre
3 µM sNPF2
ii
GRABsNPF1.0 (ΔF/Fo)
[sNPF] (µM)
B
GRABsNPF1.0 (a.u.)
Time (ZT)
21
23
1
3
5
****
***
C
Fmax (a.u.)
ns
ZT 23
ZT 3
D
GRABsNPF1.0 (F/Fmax)
ZT 3
**
CON
RNAi sNPF
E
GRABsNPF1.0 (F/Fmax)
ZT 3
*
vehicle
Cd2+
F
GRABsNPF1.0 (F/Fmax)
ZT 3
**
CON
per01

Figure 1

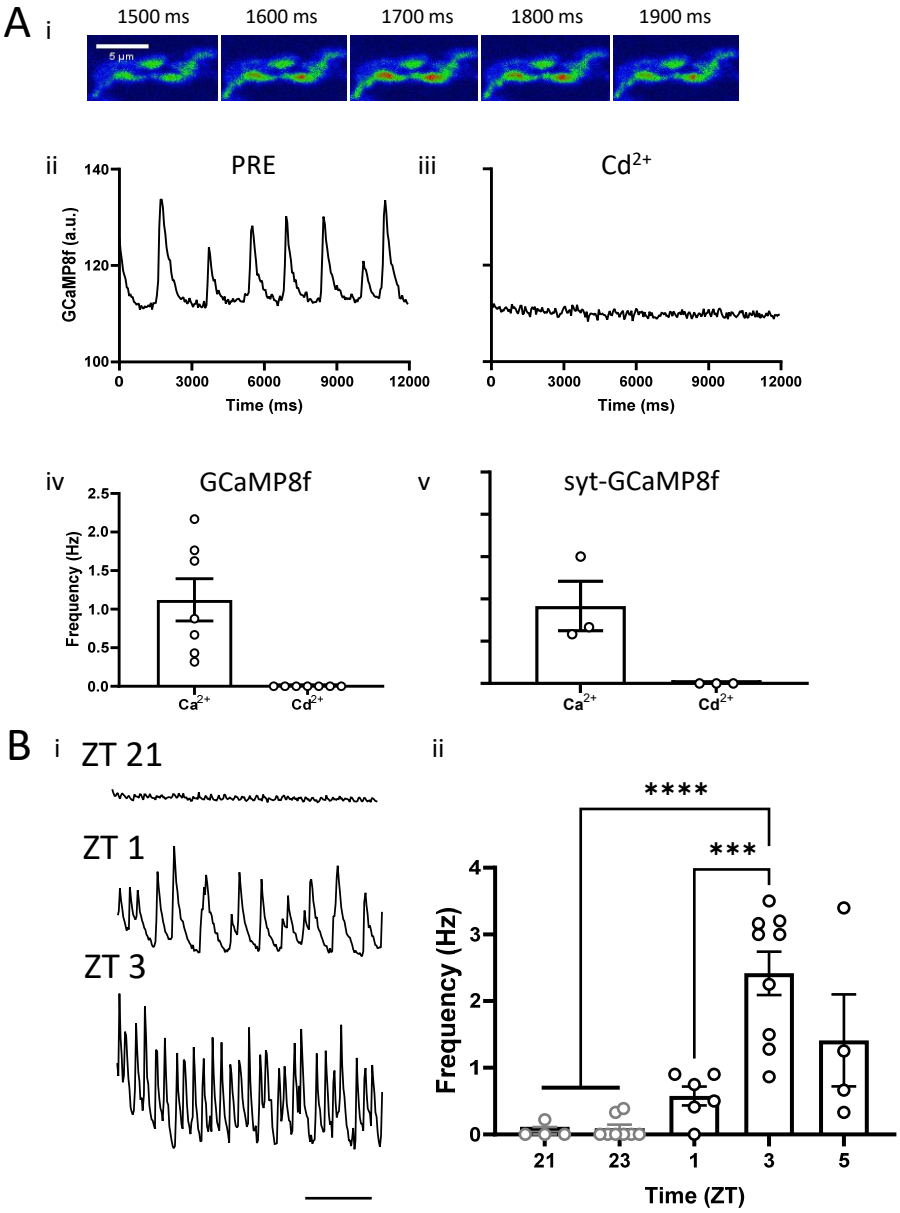
A
i
1500 ms
1600 ms
1700 ms
1800 ms
1900 ms
5 µm
ii
PRE
GCaMP8f (a.u.)
Time (ms)
iii
Cd2+
Time (ms)
iv
GCaMP8f
Frequency (Hz)
Ca2+
Cd2+
v
syt-GCaMP8f
Ca2+
Cd2+
B
i
ZT 21
ZT 1
ZT 3
ii
****
***
Frequency (Hz)
Time (ZT)

Figure 2

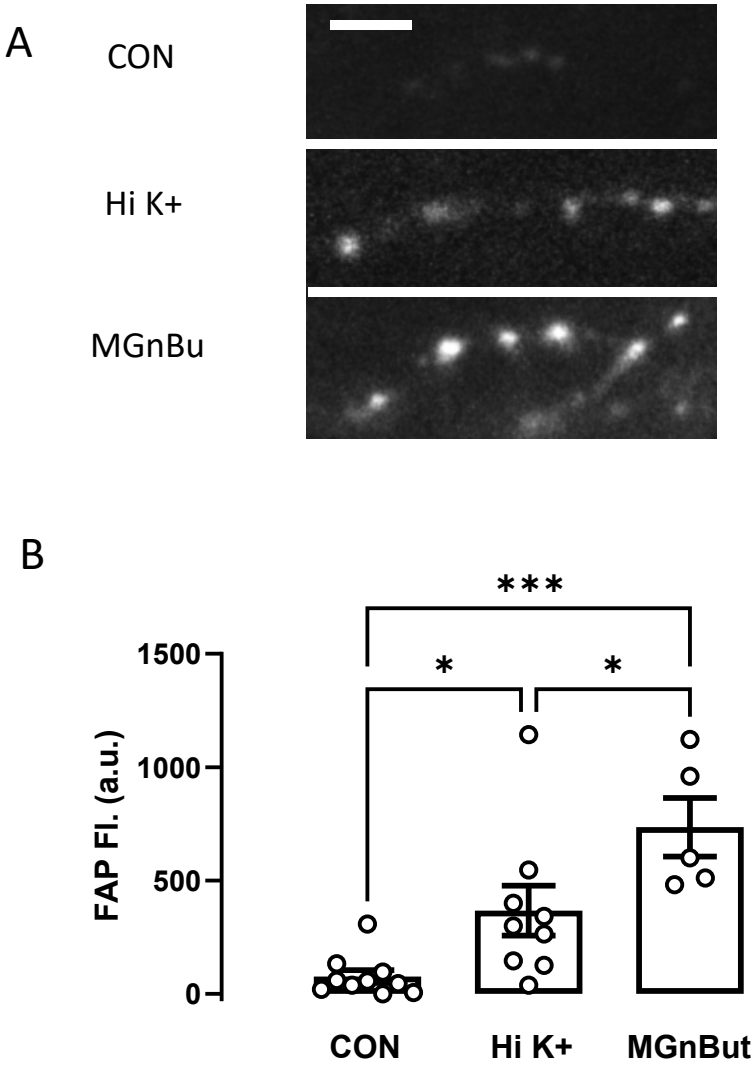

Figure 3

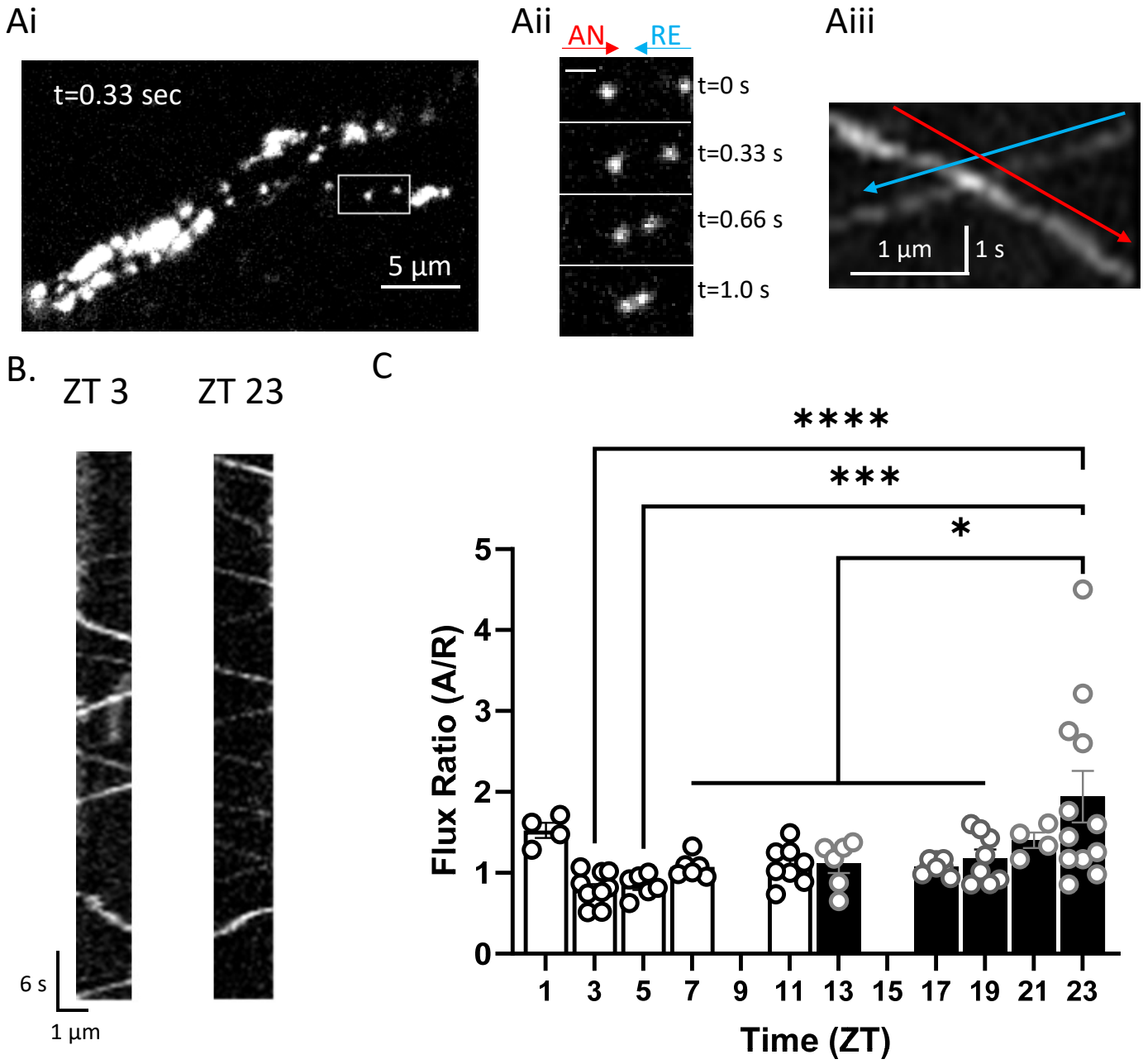
Ai
t=0.33 sec
5 µm
Aii
AN
RE
t=0 s
t=0.33 s
t=0.66 s
t=1.0 s
Aiii
1 µm
1 s
B.
ZT 3
ZT 23
6 s
1 µm
C
****
***
*
Flux Ratio (A/R)
0
1
2
3
4
5
1
3
5
7
9
11
13
15
17
19
21
23
Time (ZT)

Figure 4

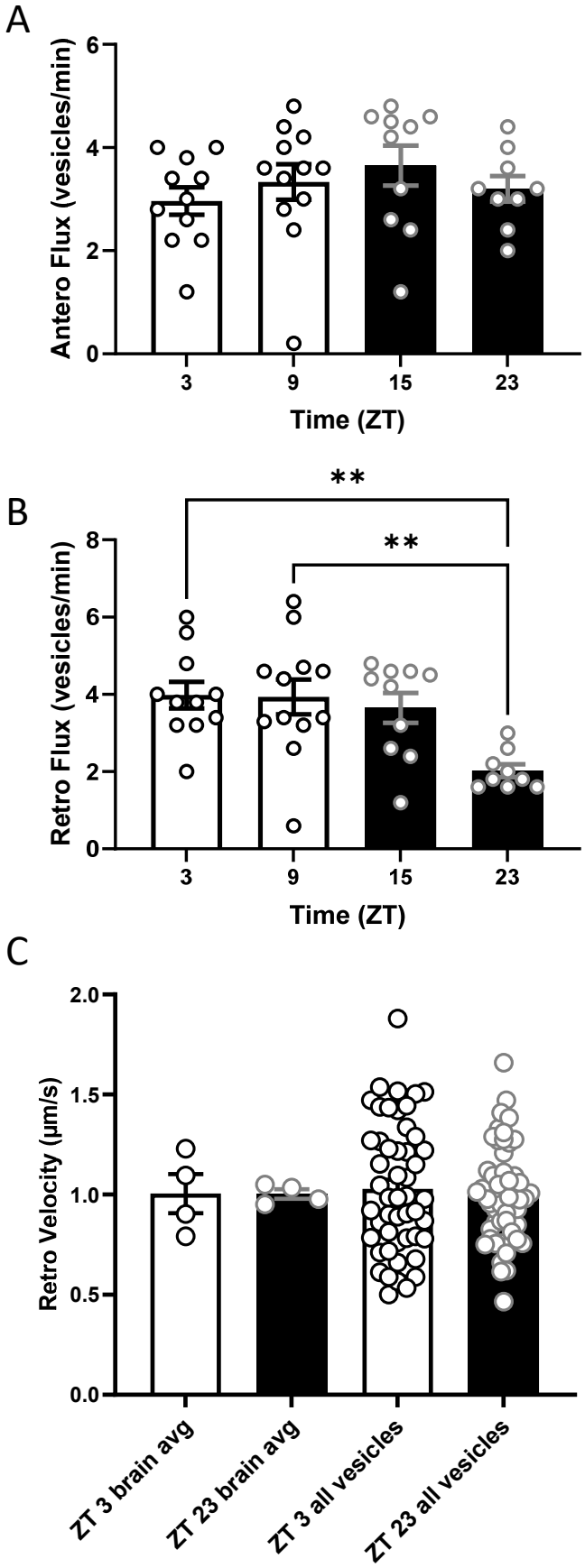
A
Antero Flux (vesicles/min)
0
2
4
6
3
9
15
23
Time (ZT)
B
**
**
Retro Flux (vesicles/min)
0
2
4
6
8
3
9
15
23
Time (ZT)
C
Retro Velocity (µm/s)
0.0
0.5
1.0
1.5
2.0
ZT 3 brain avg
ZT 23 brain avg
ZT 3 all vesicles
ZT 23 all vesicles

Figure 5

A

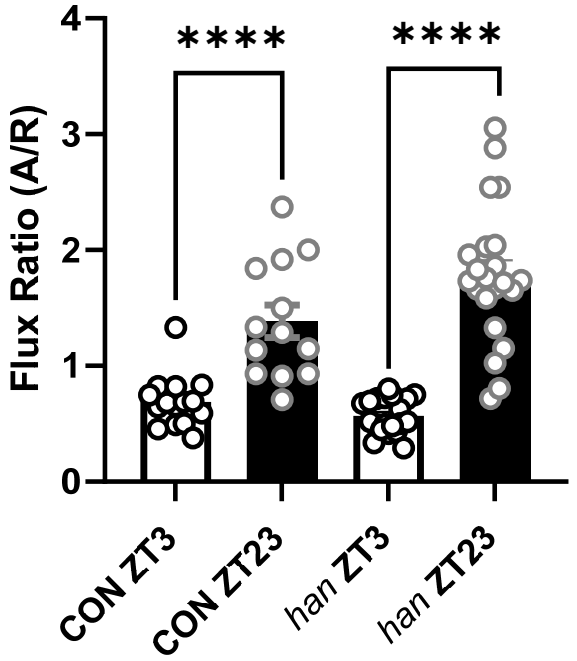
****
****
Flux Ratio (A/R)
4
3
2
1
0
CON ZT3
CON ZT23
han ZT3
han ZT23

B

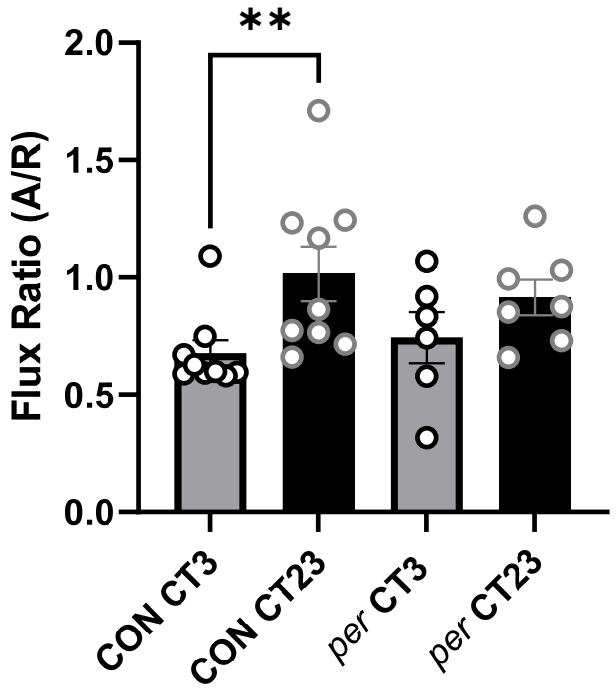
**
Flux Ratio (A/R)
2.0
1.5
1.0
0.5
0.0
CON CT3
CON CT23
per CT3
per CT23

Figure 6

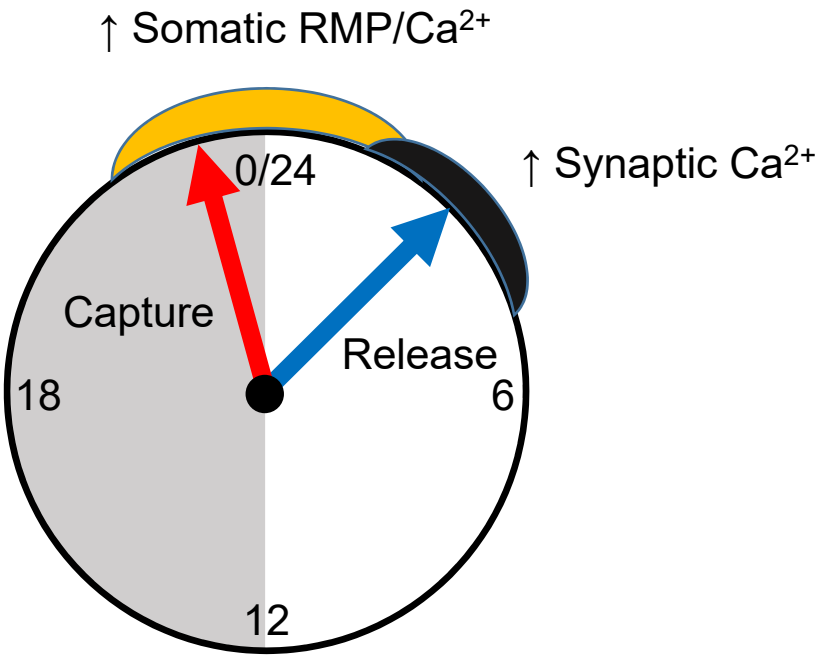

Figure 7